Cement and Concrete Research 83 (2016) 114–123

Contents lists available at ScienceDirect

Cement and Concrete Research

journal homepage: www.elsevier.com/locate/cemconres

Improvement in concrete resistance against water and chloride ingress by adding graphene nanoplatelet

Hongjian Du, Hongchen Jacey Gao, Sze Dai Pang *

Department of Civil and Environmental Engineering, National University of Singapore, 117576, Singapore

ARTICLE INFO

Article history:
Received 6 July 2015
Accepted 9 February 2016
Available online 2 March 2016

Keywords:
Durability (C)
Microstructure (B)
Pore size (B)
Tortuosity (B)
Transport properties (C)

ABSTRACT

Graphene nanoplatelet (GNP) is a cheap impermeable carbon-based nanoplatelet with large surface-to-volume ratio and has been exploited in polymer materials to improve their transport resistance. Experimental investigation on the transport properties under chloride and water exposure was carried out on concrete containing up to 2.5% of GNP at 0.5% increment. The pore structure was inferred using mercury intrusion porosimetry and significant reduction in pore sizes was measured. Concrete with 1.5% of GNP showed the greatest reduction in transport; water penetration depth, chloride diffusion, and migration coefficients were reduced by 80%, 80%, and 37%, respectively. The barrier effects of GNP were characterized and it was found that more than 50% of the improvement in transport resistance can be attributed to tortuosity while the rest to pore refinement. However, further improvement did not take place at GNP content higher than 1.5% due to limitation in dispersing the nanoplatelet clusters.

1. Introduction

Civil infrastructures are often exposed to harsh environments and severe loading conditions. For structures in aggressive environments, durability is one of the most important properties of concrete since it severely affects the service life and maintenance cost of these structures. The durability of concrete is strongly influenced by its transport properties to the harmful agents such as water, carbon dioxide (CO_2), chloride, etc. [1]. Existing durability enhancement methods mainly include (a) lowering water–cement ratio with the aid of water-reducing admixtures, (b) adding supplementary cementitious materials, and (c) using chemical admixtures such as corrosion inhibitors.

Recently, there have been increasing interests in using nanoparticles for building materials to achieve better mechanical performance and multi-functionality [2,3]. Previous studies have explored the use of nano-SiO_2 [4–11], nano-TiO_2 [11–13], nano-$CaCO_3$ [14,15], carbon-nanotube (CNT) [16–25], and carbon-nanofiber (CNF) [24–25] in cement-based materials. At the same time, there are some pioneering studies on the use of graphene oxide (GO) to reinforce the cement pastes for better mechanical properties [26–30] and durability performances [31]. GO is synthesized from natural graphite using modified Hummers method that normally involves several steps and different techniques [26–31]. Although obvious enhancement in the flexural toughness of cement paste has been reported, the limitations of low production- and low cost-effectiveness of GO are factors that limit its wide application, particularly in the cost-sensitive construction industry.

There is another promising form of nano-scale carbon-based material, the graphene nano-platelet (GNP), which has been reported to have good mechanical properties, barrier properties against liquids diffusion, and low cost. GNP has been widely studied in polymer nanocomposites [32–34] but yet to be explored in cement nanocomposites until recently [35–41]. In comparison with the 0-D shape of nano-SiO_2, nano-TiO_2, nano-$CaCO_3$ or the 1-D shape of CNT/CNF, GNP is a 2-D nano-filler, which consists of graphene layers with thickness less than 100 nm and diameter of several micrometers as shown by the scanning electron microscope (SEM) images in Fig. 1(a). The reported influences of nano-particles on the various properties of cement-based composites in terms of their representative morphologies are summarized in Table 1.

It has been reported that nano-particles can fill the voids in cement paste matrix, leading to lower porosity, higher strength, and better durability. However, it should be noted that all the beneficial influences caused by nano-particles may not realize unless being uniformly dispersed in the matrix. Otherwise, nano-particles can form agglomerates and weak pockets, leading to stress concentration which compromises the properties of the nanocomposites [40]. Up to date, research on using 2-D nano-particles to improve the durability of cementitious composites is still limited. There is a large gap in the study of the durability of cement-based material with 2-D nano-particles, which had been demonstrated to significantly reduce the permeability of polymer matrix [33,34]. Furthermore, very few studies have been conducted to investigate the properties of concrete reinforced with GNP. Du et al. [35] first reported on the use of GNP in cement mortar and studied

* Corresponding author. Tel.: +65 65162799; fax: +65 67791635.
E-mail address: ceepsd@nus.edu.sg (S.D. Pang).

http://dx.doi.org/10.1016/j.cemconres.2016.02.005

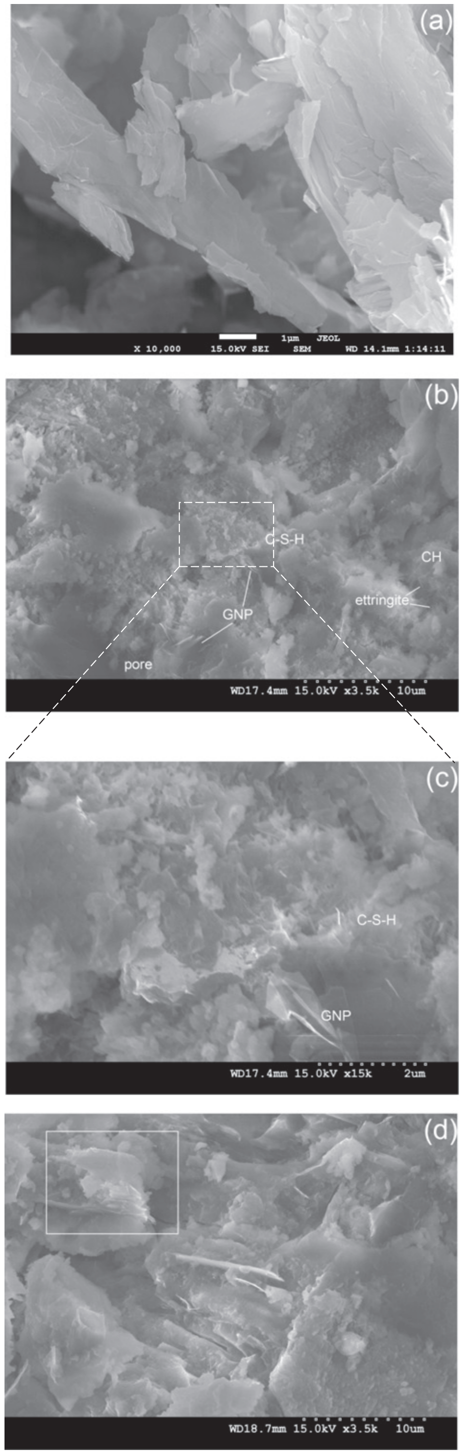

Fig. 1. SEM images of (a) as-received GNP (×10 k mag.), (b) fractured surface of GC-0.5 concrete (×3.5 k mag.), (c) close-up view (×15 k mag.), and (d) clustering of GNP in GC-2.5 concrete (×3.5 k mag.)

the effect of GNP on the transport properties. Peyvandi et al. [36] reported on the reduced water sorptivity and increased acid resistance of concrete pipes with a fixed GNP content. However, the special dry-cast technique employed in the study leaves a question on whether the same performance can be achieved for wet-cast concrete which is much more commonly used in the industry. In a recent work done by Du and Pang [40], the microstructure and transport properties of cement mortar with GNP addition of 2.5%, 5.0%, and 7.5% were studied. Significant improvement in transport resistance was measured for all mortar mixes with the largest improvement reported for the smallest dosage of GNP at 2.5%. The results seem to suggest that a dosage of GNP less than 2.5% could derive better performance but this has not been explored.

The objective of this study is to investigate the influences of GNP, for up to 2.5%, on the transport properties of concrete. The pore structure of concrete greatly governs the transport properties of concrete and is probed in this study using mercury intrusion porosimetry (MIP) to investigate the effect of this 2-D nanoplatelet. The chloride ion and water penetration have serious implications on the corrosion of steel reinforcement in concrete, and thus motivated the determination of the water permeability, chloride diffusion and migration coefficients after the addition of GNP. The pore structure and tortuosity are characterized, and comparisons between the reduction in transport properties in mortar and in concrete are made to evaluate the contributions of pore refinement and tortuosity toward barrier effects. While the focus of this paper is to examine the effect of GNP on the transport properties, the mechanical properties are also characterized to ascertain no adverse effects owing to the GNP.

2. Test program

2.1. Selection of GNP product

There are a variety of GNP products available on market, with different sizes, physical properties, and manufacturing methods. Based on the findings from reported literature [31,35,36,40,41], all GNP products are expected to enhance the cement composites resistance against water and aggressive liquids. First, the inherent impermeable nature enables graphene-based materials to be barriers to prevent ions diffusion. Second, the nanoscale thickness of GNP could accelerate cement hydration and thus densify the microstructures. Third, the layered morphology of GNP could block the interconnected pores, thus refining the pore systems. Therefore, it is plausible that GNP could increase the resistance of cement against water and chloride ions penetration. To verify it, three different GNP products were added into cement mortar and the water sorptivity was measured to characterize the resistance against ion penetration. The physical properties of GNPs are listed in Table 2. Mix proportion of the cement mortar is 0.485: 1: 2.75 for water: cement: sand. Initial water sorptivity was measured for mortar specimens at the age of 28 days, according to ASTM C 1585 [42]. More information can be found in [40]. Three specimens were tested for each mortar mix and the average values with the error ranges were displayed in Fig. 2. The water sorption was dramatically reduced by 27% to 50% and the effect is more pronounced with an increase in GNP aspect ratio. Peyvandi et al. [36], Peyvandi and Soroushian [41], and Mohammed et al. [31] all reported that the sorption rate of water would be hindered by the inclusion of GNP in the cement composites. The performance of the cement composite is dependent on the physical properties of the GNP. In this study, GNP A3775 with a representative aspect ratio in the order of 10^2 was adopted. This is also consistent with the previous work [40] where the benefits of GNP in mortar were realized. The same GNP is selected to investigate its benefits in concrete, which is the most widely used construction material.

2.2. Materials

CEM I 52.5 N cement was used in this study, with chemical composition shown in Table 3. Natural sand and coarse aggregate with maximum size of 4.75 and 19 mm, respectively, were used. Fig. 3 shows the particle size distribution (PSD) curves for both fine and coarse aggregates, as well as cement. PSD of coarse and fine aggregates were determined by standard sieve analysis. Laser scattering particle size analyzer, Malvern Mastersizer was used to determine PSD of cement. PSD of GNP was measured before and after sonication by dynamic

Table 1
Influences of carbon nano-particles on properties of cement-based materials in terms of their representative morphologies.

	Nano-SiO_2/TiO_2	CNT/CNF	GO/GNP
Morphology	Sphere (0-D)	Cylinder (1-D)	Platelet (2-D)
Typical size	7–40 nm in diameter	10–100 nm in outer diameter	0.3–100 nm in thickness
Pore-structure	Reduce the porosity because of nano-filler effect and pozzolanic reaction of nano-SiO_2 [5–9]	Decrease the porosity and refine the pore structure [17–19]	Platelets provide larger surface area for nucleation of hydration products and refine the pore structure [40].
Mechanical strength	Accelerate cement hydration and increase early-age strength [5]	Increase flexural strength and elastic modulus of paste [18,25]	Increase compressive strength of cement mortar [40]; increase elastic modulus and flexural toughness of paste [26,27,30].
Shrinkage	N.A.	Decrease autogenous shrinkage [18]	N.A.
Durability	Decrease water penetration [7]; reduce the calcium leaching rate in paste [4]; increase the resistance against chloride ingress [9,10]	N.A.	Increase the resistance of mortar to water and chloride penetration due to the refined microstructure and impermeable barrier effect [35,36,40,41]
Multi-functionality	Self-cleaning and de-polluting based on photocatalytic activity of nano-TiO_2 [11,12]	Stress and strain sensing capability of paste [16,20,21,23,24]. Increase the electromagnetic wave-shielding of mortar [22].	Damage sensing of mortar with GNP [37–39]. Piezoresistivity-based strain sensing of mortar with GNP [37,38].

light scattering (DLS) on Malvern Zetasizer Nano ZS. The principles of DLS assume the particles to be spherical. For non-spherical particle, DLS will give the effective diameter of a sphere that has the same average translational diffusion coefficient as the particle being measured. Even though DLS does no measure the actual size, it provides information for comparing the size of particles between samples [43–45]. The oven-dry unit weight and water absorption capacity of coarse aggregates were 1650 kg/m^3 and 0.8%, respectively. The SSD-specific gravity and water absorption capacity for natural sand were 2.65 and 1%, respectively. GNP was exfoliated from surface-enhanced expanded graphite flake (Grade A 3775, Asbury Graphite Mills, Inc). Its physical properties are summarized in Table 2. The mix proportion for the selected reference concrete is shown in Table 4. GNP was added at contents of 0.5, 1.0, 1.5, 2.0, and 2.5% by weight of cement.

2.3. Specimens

Prior to mixing of concrete ingredients, GNP was first ultra-sonicated with the aid of water and a naphthalene sulfonate-based surfactant (Darex Super 20, WR Grace Pte Ltd). This dispersant can disperse the agglomerates and stabilize the exfoliated GNP particles [40]. The amount of surfactant is also listed in Table 4 for each concrete mix. GNP and surfactant were dissolved in water and manually stirred 1 min. A high-power ultra-sonication horn was used to disperse this aqueous suspension for 2 h. During the sonication, a water bath was provided to cool down the horn. After the sonication, this suspension was added to the mixture of cement and aggregates and mixed in a pan mixer for 3 min. Particle size distribution for GNP was also measured before and after sonication and shown in Fig. 3. The added superplasticizer was found to be sufficient to achieve the desired workability of 100 mm in this study. The concrete was poured into steel molds and compacted on a vibration table. After casting, all the specimens were covered with a plastic sheet to prevent water loss and demolded after 24 h. The concrete specimens were cured in a fog room for 27 days before testing.

Table 2
Physical properties of GNPs.

GNP product	Density[a], ρ (g/cm^3)	Surface area[a], A (m^2/g)	Diameter[a], D (μm)	Thickness[b], t (nm)	Aspect ratio, λ	Purity, %
A 3775	2.26	23.7	8.0	37	215	98.0
M 850	2.26	13	3.6	71	50	99.5
TC 307	2.16	352	2.6	3	1000	99.9

[a] Provided by product datasheet from Asbury Graphite Mills, USA.
[b] Estimated from the surface area and density as $t = 2/A\rho$.

2.4. Test methods

Compressive and splitting tensile strength, static and dynamic elastic moduli of concrete were tested according to ASTM C 39 [46], C 496 [47], C 215 [48], and C 469 [49], respectively. Rapid chloride penetration test (RCPT), chloride diffusion coefficient, and water penetration depth were determined following ASTM C 1202 [50], NT BUILD 443 [51], and BS EN 12390-8 [52], respectively. For each concrete mix, six Φ100 × 200 mm cylinders were prepared for compressive and splitting tensile strengths as well as elastic modulus test. Three Φ100 × 50 mm cylinder discs were prepared for RCPT. Three Φ100 × 100 mm cylinders were immersed in a salt solution (185 g NaCl per liter) for 14, 56, and 90 days. At the immersion age of 14 and 56 days, one cylinder was taken out, axially split, and sprayed with 0.1 M silver nitrate solution on the fractured surface to determine the chloride ion penetration depth. One cylinder was used to determine the chloride content profile after 90 days of immersion at depths of 5, 15, 25, 35, and 45 mm. The total chloride content (acid soluble) was measured according to BS 1881-124 [53]. Two Φ100 × 200 mm cylinders were applied with a water pressure of 0.75 MPa on one end while the other surfaces were coated with epoxy. After subjecting the cylinders to 14 days of water pressure, they were split to measure the average water penetration front depth. Two 75 × 75 × 285 mm concrete prisms were used to determine the permeable void content at 28 days according to ASTM C 642 [54].

The pore structure of GNP-infused concrete at 28 days was probed using mercury intrusion porosimetry (MIP). After the compressive strength test, cubic chunks of concrete around 5 mm in dimension were chosen as samples for MIP. Samples devoid of large aggregates

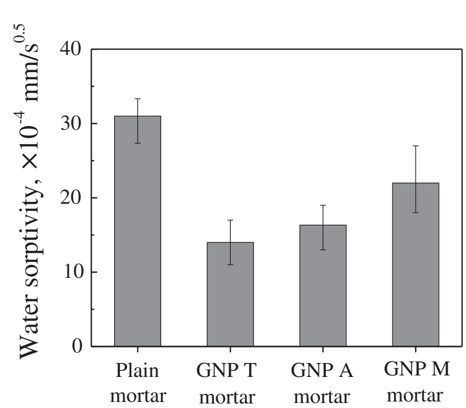

Fig. 2. Water sorptivity of cement mortar containing different GNPs at 2.5% dosage.

Table 3
Chemical composition of OPC.

Chemical composition	%
SiO_2	20.8
Al_2O_3	4.6
Fe_2O_3	2.8
CaO	65.4
MgO	1.3
SO_3	2.2
Na_2O	0.31
K_2O	0.44

Table 4
Mix proportions of concrete (kg/m^3) and slump (mm).

Mix	Water	Cement	GNP A3775	Sand	Coarse aggregate	Darex Super 20	Slump
NC	185	390	0.00	890	890	1.0	90
GC0.5	185	390	1.95	890	890	1.2	100
GC1.0	185	390	3.90	890	890	2.4	90
GC1.5	185	390	5.85	890	890	3.6	95
GC2.0	185	390	7.80	890	890	4.8	100
GC2.5	185	390	9.75	890	890	6.0	85

were extracted to ensure adequate quantity of mortar. Each MIP run requires a few cubic chunks to fill the bulb of the penetrometer; the cubic chunks were randomly sampled from different parts of the specimen to better represent the average properties [55]. Two MIP runs were carried out for each concrete mix to ensure the repeatability of the results. Due to the existence of fine aggregates and the accompanying ITZ in the samples, the interface pore structure would also be reflected by MIP results [56]. According to Laskar et al. [57], the pore size distribution determined from samples extracted away from coarse aggregates is representative of the results if the coarse aggregates were included in the MIP samples.

3. Results and discussion

3.1. Pore size distribution

The pore structure of concrete with GNP has been characterized using MIP by extracting a small sample of the cement mortar from the concrete that is devoid of coarse aggregates. The curves for the cumulative pore volume and differential distribution are shown in Fig. 4(a) and (b), respectively. With the addition of GNP, the peaks of the differential distribution curves shift toward smaller pore size, indicating a drop in the critical pore diameter. This refinement of the pore structure is attributed to the addition of GNP and similar effect in cement mortar has been demonstrated by Du and Pang [40].

The total porosity determined from the MIP test is shown in Table 5 and it should be noted that this value is not representative of the total porosity in the concrete; the presence of the interfacial transition zone (ITZ) between the cement paste and the aggregates affects the porosity but this was unaccounted for in the MIP results. By measuring the mass of saturated surface dry specimen m_{SSD}, mass of oven-dry specimen m_{OD} and mass of immersed specimen m_I, the permeable void content v_p can be determined which theoretically accounts for all the water accessible voids in the concrete:

$$v_p = \frac{m_{SSD} - m_{OD}}{m_{SSD} - m_I} \tag{1}$$

The permeable pore content for concrete with different GNP concentrations is shown in Table 5 and there was only marginal change of less than 5% when GNP was added to the concrete.

The average air void diameter, average, median, and critical pore diameters determined from MIP are shown in Table 5. With 1.0% or less of GNP added, the average air void diameter varied less than 10% but shrank significantly by more than 40% when 1.5% of GNP was added. When the amount of GNP increased further, the average air void diameter started to increase but remained smaller than the average air void diameter for the reference concrete by more than 10%. The average pore diameter also decreased when GNP is added except for the anomaly of an increase when 2.0% of GNP was added. The smallest average pore diameter was recorded for concrete with 1.5% GNP where the average pore diameter decreased by more than 20% as compared to that of the reference concrete. The same trend was observed for the median pore diameter where the smallest median pore diameter was recorded for concrete with 1.5% of GNP; the decrease in median pore diameter was more than 40% as compared to that measured in the reference concrete.

The effect of GNP on the pore structure was obvious in the critical pore diameter which shrank by at least 20% even by adding 0.5% of GNP. The changes in the critical pore diameter in concrete after addition of GNP were consistent with the results for cement mortar [40]. The critical pore size indicates the mean size of pore entryways that allows maximum percolation throughout the pore system [58] and greatly

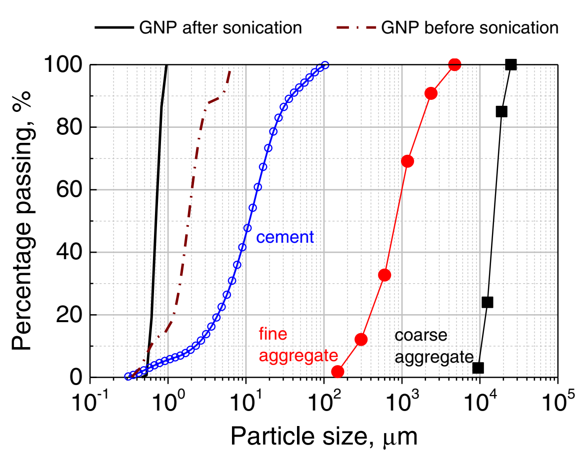

Fig. 3. Grading curves for coarse and fine aggregates, as well as cement and GNP.

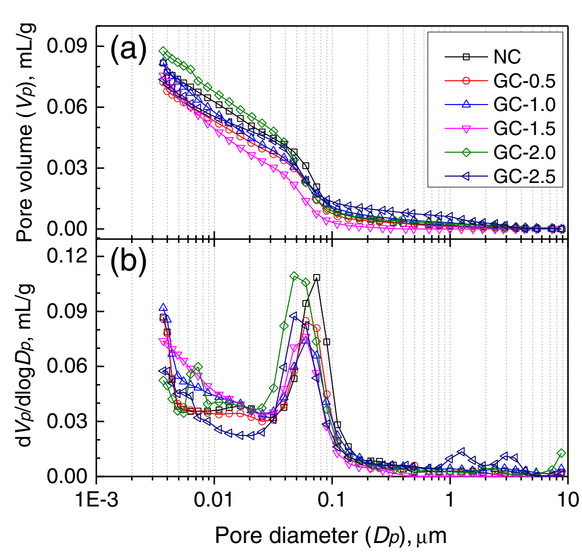

Fig. 4. Pore size investigation with MIP (a) cumulative pore volume curves; and (b) differential distribution curves.

Table 5
Pore structure of GNP infused concrete.

GNP content, %	Total porosity, %	Permeable void content, %	Average air void diameter, μm	Average pore diameter, nm	Median pore diameter, nm	Critical pore diameter, nm	Fraction of macro-pores, %
0	18.4 ± 1.7	12.0 ± 0.1	59.2 ± 1.1	17.3 ± 0.9	47.8 ± 1.3	73.8 ± 0.2	45.4 ± 1.1
0.5	16.2 ± 1.9	12.1 ± 0.0	56.3 ± 2.1	15.0 ± 0.1	36.4 ± 2.5	59.9 ± 0.2	38.2 ± 0.8
1.0	18.1 ± 1.1	11.8 ± 0.0	53.5 ± 0.9	14.6 ± 0.0	35.4 ± 1.1	59.8 ± 0.2	36.2 ± 1.4
1.5	15.8 ± 1.1	12.2 ± 0.1	34.3 ± 2.2	13.8 ± 1.0	27.2 ± 5.9	59.7 ± 0.1	31.3 ± 3.7
2.0	20.2 ± 2.6	11.9 ± 0.2	43.5 ± 2.3	18.8 ± 1.3	43.6 ± 2.5	47.7 ± 0.1	39.6 ± 1.8
2.5	16.5 ± 0.3	11.4 ± 0.4	51.7 ± 3.0	15.6 ± 1.0	37.2 ± 7.9	51.7 ± 4.1	36.0 ± 7.2

influences the transport properties of harmful fluids and gases to cement-based material [59]. It should be noted that 20% reduction in pore size does not linearly translate into a 20% reduction in permeability of cement materials. Instead, it could account for up to 80% reduction in permeability [60]. According to Mindess et al. [58], it is the macropores that can affect the transport properties of cement materials. The fraction of macropores (with diameter from 50 to 10,000 nm) for each concrete mix is also listed in Table 5. Concrete with 1.5% of GNP exhibited the lowest fraction of macropores which was 30% less than that of the reference concrete and this optimum amount of GNP with the largest effect on the fraction of macropores was consistent with the results for average and median pore diameters.

The pore structure characteristic has shown that GNP can refine the microstructure of concrete with the most significant refinement reported for 1.5% of GNP A3775. This refinement effect can be attributed to (a) the nano-filler effect which can fill and divide coarser voids into finer voids (as illustrated in Fig. 1(b) and 1(c)); and (b) providing nucleation sites for promotion of cement hydration [30] which can lead to a more homogenous microstructure when the GNP are well dispersed. However, this effect was diminished with 2.0% or more of GNP A3775 in concrete. This is due to the reduced dispersion efficiency of the sonication of GNP in a viscous suspension when the GNP concentration is high. The GNP agglomerated (shown in Fig. 1(d)) and formed porous zones when the GNP suspension is mixed with the concrete and this negated the benefits of introducing GNP into concrete.

3.2. Mechanical properties

The strength and modulus of concrete with different content of GNP are shown in Fig. 5(a) and (b), respectively. As reflected in Table 6, the null hypothesis of GNP having no effect on the mean of the mechanical properties is not rejected at 5% significance level except for the anomaly reported for the compressive strength of concrete with 1.5% of GNP. This shows that the nano-scale GNP does not benefit or adversely affect the strength and modulus of the concrete.

The compressive strength of concrete is primarily governed by the porosity of concrete and since the porosity did not vary much after introducing GNP, no significant change in the compressive strength was observed. The invariance of the flexural strength and the elastic modulus with respect to GNP content can be explained by the size of the GNP in comparison with the particle sizes in the concrete matrix. The GNPs are larger than the calcium silicate hydrate (C–S–H) particles but a few times smaller than the ITZ between the coarse aggregates and the cement matrix, which is normally 20–40 μm in thickness. While the size and aspect ratio of the GNP (as shown in Fig. 1(b)) can offer a strengthening effect on the cement paste, its size is not large enough to significantly affect the microstructure in the ITZ, or to redistribute stresses over the ITZ to mitigate the weak zones in the microstructure, or to provide adequate anchorage to bridge over the microcracks that exist between the aggregates. The null effect of GNP on the mechanical properties of concrete with coarse aggregates is consistent with earlier studies of GNP on cement with fine aggregates [40].

3.3. Resistance to chloride penetration

After 6 h of RCPT testing, the concrete samples were axially split and sprayed with 0.1 N $AgNO_3$ solution. The migration coefficient can be obtained from the measured penetration depth using the following formula [61]:

$$D_{nssm} = \frac{0.0239(273+T)L}{(U-2)t}\left[x_d - 0.0145\sqrt{\frac{(273+T)Lx_d}{U-2}}\right] \quad (2)$$

where D_{nssm} is the migration coefficient, $\times 10^{-12}$ m^2/s; T is the average temperature in the anolyte solution, °C, L is the thickness of the concrete sample, mm; U is the applied voltage, V; x_d is the average penetration depth, mm; and t is the test duration, h.

The chloride migration coefficients for concrete containing various GNP contents are displayed in Fig. 6(a). The addition of as little as 0.5% GNP could reduce the chloride migration coefficient by 25% while concrete with 1.5% GNP could reduce the chloride migration by 37% as compared to the reference concrete. The better chloride migration resistance could be attributed to the refinement in pore distribution in cement

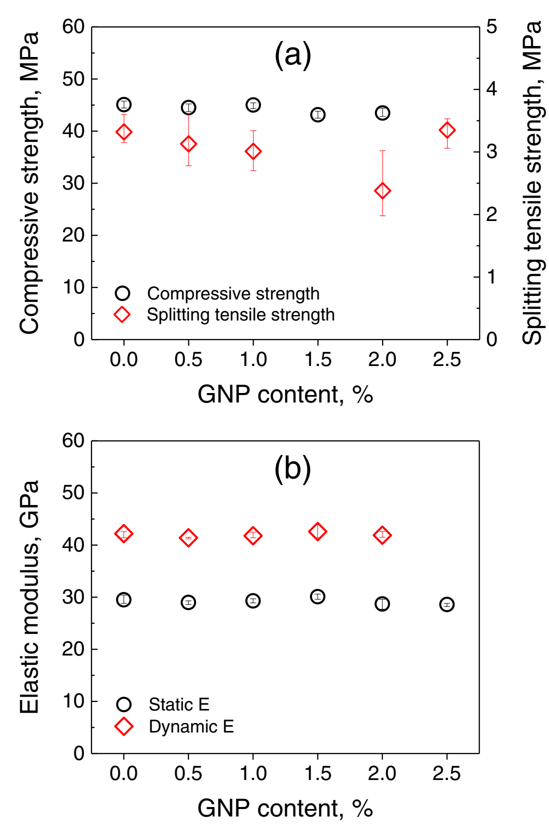

Fig. 5. Mechanical properties of concrete with GNP.

Table 6
Evaluation of the effect of GNP on mechanical properties using p-values from t-tests.

GNP content, %	Compressive strength, MPa		Splitting tensile strength, MPa		Static elastic modulus, GPa		Dynamic elastic modulus, GPa	
	Mean	p-value	Mean	p-value	Mean	p-value	Mean	p-value
0	45.1	–	3.32	–	29.5	–	42.2	–
0.5	44.5	0.393	3.13	0.546	29.0	0.389	41.4	0.180
1.0	45.0	0.909	3.01	0.243	29.3	0.773	41.8	0.493
1.5	43.1	0.023	–	–	30.1	0.358	42.6	0.608
2.0	43.5	0.059	2.38	0.077	28.7	0.827	41.9	0.602
2.5	–	–	3.35	0.890	28.6	0.178	–	–

paste which is reflected in the changes in average, median, and critical pore diameters, and fraction of macropores. Although the influence of refined pore structure was not significant in increasing mechanical strength, it contributed to improved barrier properties. At the same time, the added GNP can be considered as impermeable barriers inside the cement paste, which increase the tortuosity and decrease the pore connectivity for ingressive ions to penetrate through. However, at higher GNP concentrations, the GNP suspension became increasingly viscous, resulting in lower energy transfer within the suspension during sonication. The poorer dispersion resulted in clustering of the GNP, which does not allow the full benefits of adding GNP to be realized. It is hypothesized that the transport resistance can be further improved with more GNP, provided that the GNP can be well dispersed; further attempts are being carried out toward achieving better dispersion at higher concentrations of GNP.

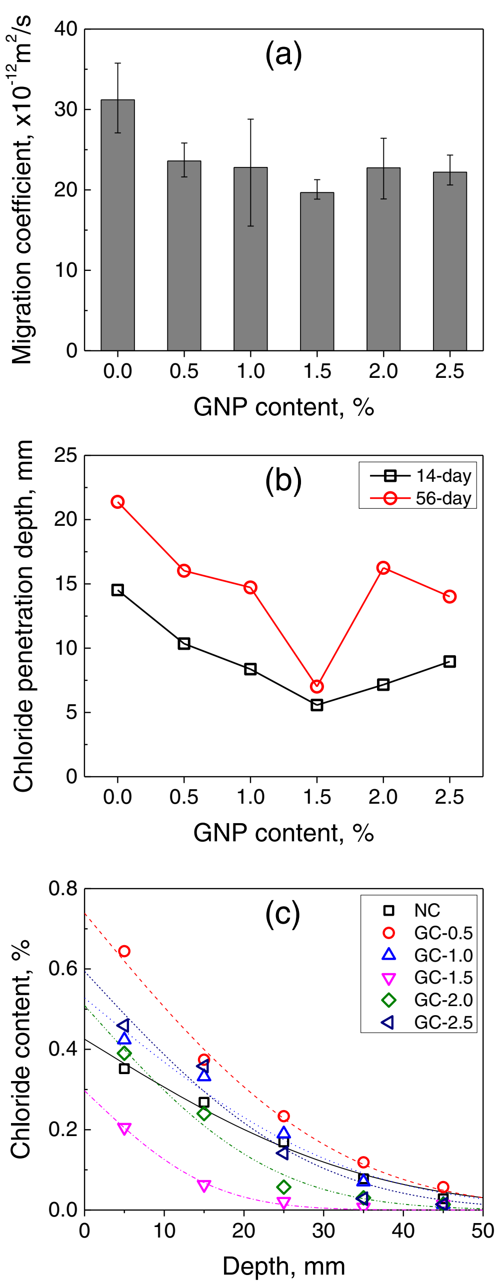

Fig. 6. Test results for concrete with GNP (a) chloride migration coefficient, (b) chloride penetration depth, and (c) chloride content profiles and best-fitted curves.

Fig. 6(b) shows the chloride ion penetration depth at 14 and 56 days. The chloride ion penetration depth increased with time from 14 to 56 days and decreased with increasing GNP content of up to 1.5%, and increased thereafter. The chloride ion penetration depth for 14 and 56 days were both reduced by about 60–70% for concrete with 1.5% of GNP as compared to the reference concrete. This is consistent with the effect of GNP concentration on chloride migration coefficient. The pathways for chloride ion to diffuse into concrete were refined in size and obstructed by the added GNP. Exceeding 1.5% GNP, the agglomeration of GNP into porous clusters would result and this led to more porous pathways for chloride ions to penetrate.

The chloride content profiles for concrete with GNP are shown in Fig. 6(c). The diffusion of chloride ions into concrete can be described by Crank's solution to Fick's second law:

$$C(x,t) = C_0\left[1 - \mathrm{erf}\left(\frac{x}{2\sqrt{D_e t}}\right)\right] \tag{3}$$

where $C(x,t)$ is the chloride content at depth x (mm) and time t (s), C_0 is the chloride content at the surface, and *erf* is the error function, D_e is the chloride diffusion coefficient, $\times 10^{-12}$ m^2/s. The best-fitted curves and the parameters for each fitted curve are displayed in Fig. 6(c) and Table 7, respectively. The chloride diffusion coefficient decreased with GNP content until up to 1.5% of GNP, indicating an enhanced impermeability which was likely due to pore refinement and barrier effect of GNP. At 1.5% of GNP, the chloride diffusion coefficient dropped by 80% as compared to the reference concrete. At higher GNP content, the dispersion will be harder, resulting in clusters which formed porous zones and this reduced the barrier effect; this phenomenon is consistent with the results for pore distribution and chloride migration coefficient.

3.4. Resistance to water penetration

The effect of GNP on water penetration depth in concrete is shown in Fig. 7. At low GNP content of 1.0% or less, the water penetration depth was not much affected which was supported by p-values of 0.45 and 0.14, for 0.5% and 1.0% of GNP, respectively. When GNP content increased to 1.5%, the water penetration depth decreased by 80% (shown in Fig. 8). This drastic drop at 1.5% of GNP was also observed in the average and median pore diameters which shrank most significantly at 1.5% of GNP. Further addition of GNP beyond 1.5% did not further reduce the water penetration depth. A similar finding has also been reported by Quercia et al. [10], in which the water permeability

Table 7
Parameters for the best-fitted curves of chloride content profiles.

Mix	D_e, $\times 10^{-12}$ m^2/s	C_0, wt.%	R^2
NC	49.7	0.43	0.981
GC0.5	38.7	0.74	0.987
GC1.0	42.6	0.53	0.963
GC1.5	10.0	0.30	0.985
GC2.0	21.5	0.51	0.975
GC2.5	31.4	0.59	0.946

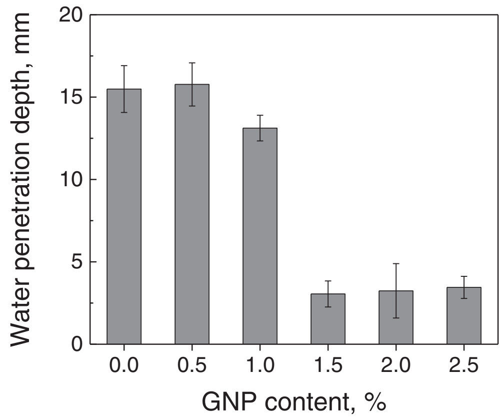

Fig. 7. Water penetration depth of GNP infused concrete.

of concrete was abruptly reduced by the addition of 3.75% nano-silica though the total water permeable porosity maintained almost the same. Compared with the previous work by Ji [7] where the water penetration depth reduced by 45% for concrete with 3.5% nano-silica (wt.% of cement), it is noted that addition of GNP is able to reduce the permeability of concrete more significantly with a smaller amount of nano-particles (1.5% GNP A3775 in this study). This can be attributed to the platelet form of the GNP which increased the tortuosity and refine the pore structure, both of which increased the resistance against water ingress as compared to the spherical nano-silica.

3.5. Mechanism of transport barrier by GNP

The experiments have shown that the pore structure in the cement paste matrix of concrete can be refined by GNP addition. This is reflected in the MIP results where the average, median, and critical pore sizes are all reduced. Besides the influence on pore structure of concrete, improvement in durability of concrete is reflected in the transport properties where the water penetration depth, chloride diffusion coefficient, and chloride migration coefficient diminished when GNP was added. This can be attributed to the refinement of capillary pore system and the barriers formed by the impermeable GNP which led to more tortuous paths for the ingress of water and chloride ions. The contribution of the two mechanisms toward the reduction in the transport properties can be estimated by evaluating the approximate tortuosity that the GNP brings about.

The contribution of tortuosity in reducing the transport of water can be evaluated by first considering the tortuosity factor τ_{2D} of evenly

Fig. 8. Test results for water penetration depth into concrete without and with 1.5% GNP.

spaced 2-D GNP in cement matrix with their planes aligned perpendicular to the direction of water ingress as expressed as follows:

$$\tau = 1 + \frac{l}{2T} \tag{4}$$

where l is the length of the nanoplatelet and T is the thickness of the unit cell. For other orientation of the nanoplatelet, the tortuosity factor can be modified with the order parameter S [62,63]:

$$\tau_{orient} = 1 + \frac{l}{2T}\left(\frac{2}{3}\right)\left(S + \frac{1}{2}\right) \tag{5}$$

If the nanoplatelets are randomly distributed, S takes the value of 0 [62,63] and the tortuosity factor can be expressed as

$$\tau_{rand} = 1 + \frac{l}{6T} \tag{6}$$

The thickness T of the unit cell depends on the dispersion distance. A simple approximation is to assume that platelets are dispersed in 1D (refer to Fig. 9(a)) with the in-plane distance between the nanoplatelets being zero while the out-of-plane distance is proportional to the volume fraction ϕ_p of platelets such that the unit cell thickness $T = t/\phi_p$ where t is the thickness of the nanoplatelet. This leads to a tortuosity factor which is commonly used by other researchers [64,65]:

$$\tau_{rand,disp1D} = 1 + \left(\frac{l}{t}\right)\left(\frac{\phi_p}{6}\right) \tag{7}$$

If the nanoplatelets are assumed to be evenly dispersed in 3D (refer to Fig. 9(b)) with a spacing of s for both in-plane and out-of-plane directions, the tortuosity factor will be larger with an amplification factor $(1 + s/l)^2$. This leads to an upper bound of the tortuosity factor for random 2D platelets.

$$\tau_{rand,disp3D} = 1 + \left(\frac{l}{t}\right)\left(\frac{\phi_p}{6}\right)\left(1 + \frac{s}{l}\right)^2 \tag{8}$$

The spacing s can be found by relating the volume of the nanoplatelet to the volume of the unit cell given below:

$$\phi_p = \frac{l^2 t}{(l+s)^2 (t+s)} \tag{9}$$

Water permeability coefficient (K_w) of concrete can be estimated from the following equation developed by Valenta [66], based on the water penetration depth (d) under water pressure (h) for the test period (t).

$$K_w = \frac{d^2 v}{2ht} \tag{10}$$

where v is the porosity of concrete. From Eq. (10), we can modify the permeability of particle-unfilled concrete with the tortuosity factor to evaluate the effect of tortuosity in particle-filled concrete: $K_w' = K_w/\tau^2_{rand,disp3D}$. This theoretical estimate of the permeability ratio K'_w/K_w is compared with the experimentally measured ratio in Fig. 10(a) where K'_w and K_w are the water permeabilities of the concrete with and without GNP, respectively. The tortuosity effect alone overestimates the decrease in water permeability for GNP at 1.0% or less as the tortuosity model illustrated in Fig 9(b) gives an upper bound estimate of the tortuosity effect. For GNP of 1.5% and above, the tortuosity effect contributes about 50% reduction in water penetration depth for concrete while the rest can be attributed to the pore refinement by the GNP. The results are consistent with the water penetration depth

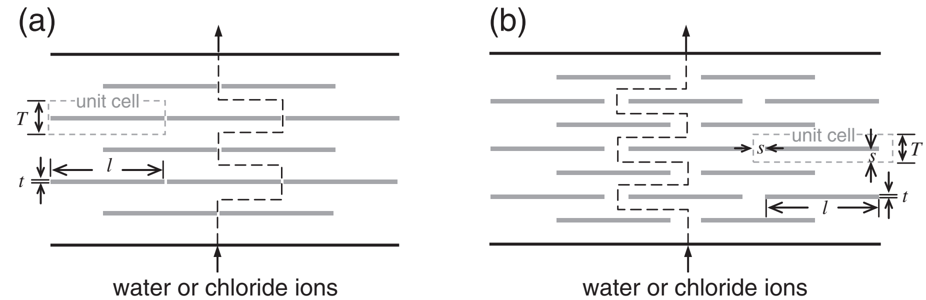

Fig. 9. Simple tortuosity-based model to describe flow of water or chloride ions through cement matrix filled with GNPs (a) uniform dispersion in 1D (b) uniform dispersion in 3D.

reported for mortar with GNP [40] where the lowest tested GNP content of 2.5% resulted in a significant drop in water penetration depth.

The ingress of chloride ions by diffusion is described by the solution to Fick's second law of diffusion in Eq. (3). If the distance x travelled by the chloride ions from the exposed surface takes into account the length of the tortuous path such that $x' = \tau_{rand,disp3D}x$, it results in an apparent chloride diffusion coefficient D' which can be expressed as [40]:

$$D_c' = D_c / \tau^2_{rand,disp3D} \tag{11}$$

This modification of D_c is based on tortuosity argument only and if we plot D_c'/D_c, we can evaluate the relative contribution of tortuosity in the chloride diffusion barrier. From the comparison of D_c'/D_c against $1/\tau^2_{rand,disp3D}$, tortuosity alone can account for the changes in chloride diffusion coefficients for GNP of 1.0% and below. At 1.5% of GNP, about half of the drop in the chloride diffusion coefficient can be explained by the increase in tortuosity while the rest can be attributed to pore refinement and that is consistent with the smallest pore diameter reported for 1.5% of GNP. As the GNP content increased beyond 1.5%, the pore refinement effect diminished which was expected based on the trends for the average air void diameter and median pore diameter at those GNP contents.

The non-steady state migration coefficient of chloride ions under an applied potential difference can be described by Eq. (2). Similar to the treatment of chloride diffusion coefficient, we can evaluate the contribution of tortuosity to the non-steady state migration coefficient by comparing D_{nssm}'/D_{nssm} against $1/\tau^2_{rand,disp3D}$ [40] as shown in Fig. 10(b). We can expect tortuosity alone to contribute almost fully to the chloride diffusion barrier for different GNP contents. At GNP content of 2.0% and higher, the D_{nssm}'/D_{nssm} ratio raises and this is likely due to the presence of GNP clusters.

The efficiency of GNP of blocking the transport of water and chloride ions in cement mortar was investigated by Du and Pang [40] recently, in which GNP was added at contents of 0, 2.5%, 5.0%, and 7.5% by weight of cement. It was reported that the addition of 2.5% GNP could provide the highest barrier efficiency due to the pore refinement and increased tortuosity in the matrix. However, the performances of cement composites with GNP dosage less than 2.5% were not investigated. Fig. 11 shows a comparison of the relative water permeability and chloride ingress before and after the addition of GNP in cement composites, collected from previous work [40], and this study. Compared to the reference plain cement composites, the use of GNP hinder the transport of water and chloride ions, demonstrating the function as barriers. Also, this barrier efficiency does not consistently increase with higher GNP amount while 1.5% of GNP seems to be the optimum due to the limitation of the current processing method to further disperse the GNP clusters at higher percentage.

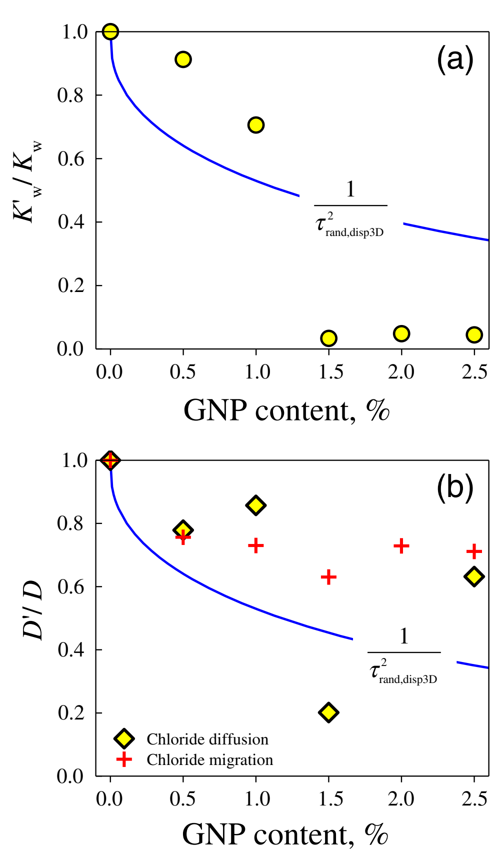

Fig. 10. Comparisons between the theoretical prediction of the 2-D barrier effect of GNP and experimental observations on (a) water permeability, and (b) chloride diffusion and migration.

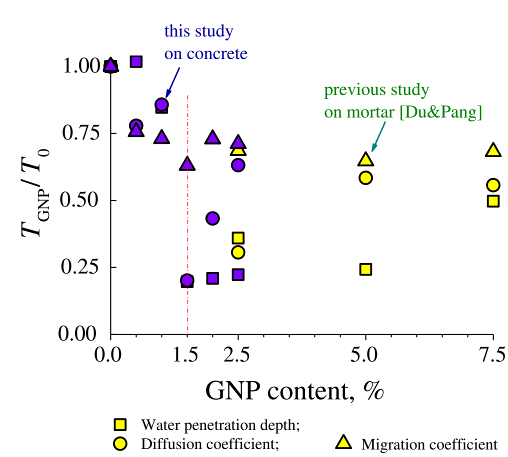

Fig. 11. Comparisons between this study and previous work on the barrier efficiency of GNP in cement composites.

4. Conclusions

The mechanical and transport properties of concrete infused with a low-cost 2D nano-platelet, GNP, were investigated experimentally. The following conclusions can be obtained:

1. The porosity did not vary much with the addition of GNP which does not change the compressive strength. The size of the GNP is significantly smaller than the ITZ between the cement paste and aggregates, rendering it ineffective to increase the flexural strength or the modulus.
2. The addition of GNP helped in pore refinement of the cement paste; the average, median and critical pore diameters, and the average void diameter are all reduced due to the nano-filler and segmentation effect of GNP on the capillary pores.
3. This is the first study to characterize the influence of 2-D nano-filler on the durability performance of concrete. It is found that GNP improves the resistance of concrete to chloride ion and water penetration, attributed to the refined microstructure and increased tortuosity of concrete. 1.5% of GNP A3775 was found to be the optimum content for current processing method to improve the durability performance of concrete. At this optimal GNP content, the water permeability, chloride diffusion coefficient, and chloride migration coefficient were reduced by 80%, 80%, and 40%, respectively.
4. Despite the presence of more and larger ITZ with the introduction of coarse aggregates into the cement matrix, the effectiveness of the GNP in reducing the transport of the water and chloride ions does not seem to be affected. The results support the use of GNP with the proposed processing method as a means of enhancing the durability of concrete.

Acknowledgments

The authors wish to express their thanks to A*STAR SERC (grant number R-302-000-034-305) for the financial support. The GNP material supply from Asbury Graphite Mills, USA, is acknowledged. The authors are grateful to Prof. Zhang Yong and his research fellow Ms. NM Idris for their help in characterizing the GNP particle size distribution.

References

[1] A.M. Neville, Properties of Concrete, fifth ed. Pearson, Essex, 2011.
[2] K. Sovolev, M. Ferrada-Gutierrez, How nanotechnology can change the concrete world: part I, Amer. Ceram. Soc. Bull. 84 (2005) 14–17.
[3] F. Sanchez, K. Sobolev, Nanotechnology in concrete – a review, Constr. Build. Mater. 24 (2010) 2060–2071.
[4] J.J. Gaitero, I. Campillo, A. Guerrero, Reduction of the calcium leaching rate of cement paste by addition of silica nanoparticles, Cem. Concr. Res. 29 (2008) 1112–1118.
[5] P. Hou, S. Kawashima, D. Kong, D.J. Corr, J. Qian, S.P. Shah, Modification effects of colloidal nanoSiO_2 on cement hydration and its gel property, Compos. Part B 45 (2013) 440–448.
[6] H. Li, H. Xiao, J. Yuan, J. Ou, Microstructure of cement mortar with nano-particles, Compos. Part B 35 (2004) 185–189.
[7] T. Ji, Preliminary study on the water permeability and microstructure of concrete incorporating nano-SiO_2, Cem. Concr. Res. 35 (2005) 1943–1947.
[8] P. Hou, J. Qian, X. Cheng, S.P. Shah, Effects of the pozzolanic reactivity of nanoSiO_2 on cement-based materials, Cem. Concr. *compos*. 55 (2015) 250–258.
[9] H. Du, S.D. Pang, Effect of colloidal nano-silica on the mechanical and durability performance of mortar, Key Eng. Mater. 629 (2014) 443–448.
[10] G. Quercia, P. Spiesz, G. Husken, H.J.H. Brouwers, SCC modification by use of amorphous nano-silica, Cem. Concr. *compos*. 45 (2014) 69–81.
[11] L. Senff, D.M. Tobaldi, S. Lucas, D. Hotza, V.M. Ferreira, J.A. Labrincha, Formulation of mortars with nano-SiO_2 and nano-TiO_2 for degradation of pollutants in buildings, Compos. Part B 44 (2013) 40–47.
[12] P. Krishnan, M.-H. Zhang, L. Yu, H. Feng, Photocatalytic degradation of particulate pollutants and self-cleaning performance of TiO_2-containing silicate coating and mortar, Constr. Build. Mater. 44 (2013) 309–316.
[13] H. Li, H. Xiao, X. Guan, Z. Wang, L. Yu, Chloride diffusion in concrete containing nano-TiO_2 under coupled effect of scouring, Compos. Part B 56 (2014) 698–704.
[14] S. Kawashima, J.W.T. Seo, D. Corr, M.C. Hersam, S.P. Shah, Dispersion of $CaCO_3$ nanoparticles by sonication and surfactant treatment for application in fly ash-cement systems, Mater. Struct. 47 (2014) 1011–1023.
[15] W. Li, Z. Huang, T. Zu, C. Shi, W.H. Duan, S.P. Shah, Influence of Nanolimestone on the Hydration, Mechanical Strength, and Autogenous Shrinkage of Ultrahigh-Performance Concrete, J. Mater. Civ, Eng, 2015, http://dx.doi.org/10.1061/(ASCE)MT.1943-5533.0001327.
[16] F. Azhari, N. Banthia, Cement-based sensors with carbon fibers and carbon nanotubes for piezoresistive sensing, Cem. Concr. *compos*. 34 (2012) 866–873.
[17] F. Collins, J. Lambert, W.H. Duan, The influence of admixtures on the dispersion, workability, and strength of carbon nanotube-OPC paste mixtures, Cem. Concr. *compos*. 34 (2012) 201–207.
[18] M.S. Konsta-Gdoutos, Z.S. Metaxa, S.P. Shah, Multi-scale mechanical and fracture characteristics and early-age strain capacity of high performance carbon nanotube/cement nanocomposites, Cem. Concr. *compos*. 32 (2010) 110–115.
[19] G.Y. Li, P.M. Wang, X. Zhao, Mechanical behavior and microstructure of cement composites incorporating surface-treated multi-walled carbon nanotubes, Carbon 43 (2005) 1239–1245.
[20] G.Y. Li, P.M. Wang, X. Zhao, Pressure-sensitive properties and microstructure of carbon nanotube reinforced cement composites, Cem. Concr. *compos*. 29 (2007) 377–382.
[21] A.L. Materazzi, F. Ubertini, A. D'Alessandro, Carbon nanotube cement-based transducers for dynamic sensing of strain, Cem. Concr. *compos*. 37 (2013) 2–11.
[22] I.W. Nam, H.K. Lee, J.B. Sim, S.M. Choi, Elctromagnetic characteristics of cement matrix materials with carbon nanotubes, ACI Mater. J. 109 (2012) 363–370.
[23] B. Han, K. Zhang, X. Yu, E. Kwon, J. Ou, Electrical characteristics and pressure-sensitive response measurement of carboxyl MWNT/cement composites, Cem. Concr. *compos*. 34 (2012) 794–800.
[24] M.S. Konsta-Gdoutos, C.A. Aza, Self-sensing carbon nanotube (CNT) and nanofiber (CNF) cementitious composites for real time damage assessment in smart structures, Cem. Concr. *compos*. 53 (2014) 162–169.
[25] B.M. Tyson, R.K.A. Al-Rub, A. Yazadanbakhsh, Z. Graslev, Carbon nanotubes and carbon nanofibers for enhancing the mechanical properties of nanocomposite cementitious materials, J. Mater. Civ. Eng. 23 (2011) 1028–1035.
[26] M. Saafi, L. Tang, J. Fung, M. Rahman, J. Liggat, Enhanced properties of graphene/fly ash geopolymeric composite cement, Cem. Concr. Res. 67 (2015) 292–299.
[27] K. Gong, Z. Pang, A.H. Korayem, L. Qiu, D. Li, F. Collins, C.M. Wang, W.H. Duan, Reinforcing effects of graphene oxide on Portland cement paste, J. Mater. Civ. Eng. 27 (2015), A4014010.
[28] Z. Pan, L. He, L. Qiu, A.H. Korayem, G. Li, J.W. Zhu, F. Collins, D. Li, W.H. Duan, C.M. Wang, Mechanical properties and microstructure of a graphene oxide-cement composite, Cem. Concr. *compos*. 58 (2015) 140–147.
[29] S. Lv, Y. Ma, C. Qiu, T. Sun, J. Liu, Q. Zhou, Effect of graphene oxide nanosheets of microstructure and mechanical properties of cement composites, Constr. Build. Mater. 49 (2013) 121–127.
[30] E. Horszczaruk, E. Mijowska, R.J. Kalenczuk, M. Aleksandrzak, S. Mijowska, Nanocomposite of cement/graphene oxide – impact on hydration kinetics and Young's modulus, Constr. Build. Mater. 78 (2015) 234–242.
[31] A. Mohammed, J.G. Sanjayan, W.H. Duan, A. Nazari, Incorporating graphene oxide in cement composites: a study of transport properties, Constr. Build. Mater. 84 (2015) 341–347.
[32] B.Z. Jang, A. Zhamu, Processing of nanographene platelet (NGPs) and NGP nanocomposites: a review, J. Mater. Sci. 43 (2008) 5092–5101.
[33] O.C. Compton, S. Kim, C. Pierre, J.M. Torkelson, S.T. Nguyen, Crumpled graphene nanosheets as highly effective barrier property enhancers, Adv. Mater. 22 (2010) 4759–4763.
[34] J.R. Potts, D.R. Dreyer, C.W. Bielawski, R.S. Ruoff, Graphene-based polymer nanocomposites, Polymer 52 (2011) 5–25.
[35] H. Du, S.D. Pang, S.T. Quek, Transport Properties of Cement Mortar with Graphite Nanoplatelet, in: 20th International Conference on Composites/Nano Engineering, Beijing, China, 2012.
[36] A. Peyvandi, P. Soroushian, A.M. Balachandra, K. Sobolev, Enhancement of the durability characteristics of concrete nanocomposites pipes with modified graphite nanoplatelets, Constr. Build. Mater. 47 (2013) 111–117.
[37] H. Du, S.T. Quek, S.D. Pang, Smart multifunctional cement mortar containing graphite nanoplatelet, in: J.P. Lynch, C.B. Yun, K.W. Wang (Eds.), SPIE, vol. 8692, SPIE Press, San Diego, USA 2013, p. 869223, http://dx.doi.org/10.1117/12.2009005.
[38] S.D. Pang, H.J. Gao, C. Xu, S.T. Quek, H. Du, Strain and damage self-sensing cement composites with conductive graphene nanoplatelet, in: J.P. Lynch, K.W. Wang, H. Sohn (Eds.), SPIE, vol. 9061, SPIE Press, San Diego, USA 2014, p. 9061126, http://dx.doi.org/10.1117/12.2045329.
[39] J.-L. Le, H. Du, S.D. Pang, Use of 2-D graphene nanoplatelets (GNP) in cement composites for structural health evaluation, Compos. Part B 67 (2014) 555–563.
[40] H. Du, S.D. Pang, Enhancement of barrier properties of cement mortar with graphene nanoplatelet, Cem. Concr. Res. 76 (2015) 10–19.
[41] A. Peyvandi, P. Soroushian, Structural performance of dry-cast concrete nanocomposite pipes, Mater. Struct. 48 (2015) 461–470.
[42] ASTM C 1585, Standard Test Method for Measurement of Rate of Absorption of Water by Hydraulic-Cement Concretes, ASTM International, West Conshohocken, PA, 2004.
[43] S. Stankovich, R.D. Piner, S.T. Nguyen, R.S. Ruoff, Synthesis and exfoliation of isocyanate-treated graphene oxide nanoplatelet, Carbon 44 (2006) 3342–3347.
[44] J. Lu, I. Do, H. Fukushima, I. Lee, L.T. Drzal, Stable aqueos suspension and self-assembly of graphite nanoplatelet coated with various polyelectrolytes, J. Nanomater. 186486 (2010).
[45] M. Lotya, A. Rakovich, J.F. Donegan, J.N. Coleman, Measuring the lateral size of liquid-exfoliated nanosheets with dynamic light scattering, Nanotechnol. 24 (2013) 265703.
[46] ASTM C 39, Standard Test Method for Compressive Strength of Cylindrical Concrete Specimens, ASTM International, West Conshohocken, PA, 2005.
[47] ASTM C 496, Standard Test Method for Splitting Tensile Strength of Cylindrical Concrete Specimens, ASTM International, West Conshohocken, PA, 2004.

[48] ASTM C 215, Standard Test Method for Fundamental Transverse, Longitudinal, and Torsional Resonant Frequencies of Concrete Specimens, ASTM International, West Conshohocken, PA, 2008.
[49] ASTM C 469, Standard Test Method for Static Modulus of Elasticity and Poisson's Ratio of Concrete in Compression, ASTM International, West Conshohocken, PA, 2002.
[50] ASTM C 1202, Standard Test Method for Electrical Indication of Concrete's Ability to Resist Chloride Ion Penetration, West Conshohocken, PA, 2005.
[51] NT BUILD 443, Concrete, Hardened: Accelerated Chloride Penetration, NORDTEST, Espoo, 1995.
[52] BS EN 12390-8, Testing Hardened Concrete Part 8: Depth of Penetration of Water Under Pressure, British Standard Institute, London, 2009.
[53] BS 1881-124, Testing Concrete-Part 124: Method for Analysis of Hardened Concrete, British Standard Institute, London, 1998.
[54] ASTM C 642, Standard Test Method for Density, Absorption, and Voids in Hardened Concrete, ASTM International, West Conshohocken, PA, 1997.
[55] R. Kumar, B. Bhattacharjee, Study on some factors affecting the results in the use of MIP method in concrete research, Cem. Concr. Res. 33 (2003) 417–424.
[56] D.N. Winslow, M.D. Cohen, D.P. Bentz, K.A. Snyder, E.J. Garboczi, Percolation and pore structure in mortar and concrete, Cem. Concr. Res. 24 (1994) 25–37.
[57] A.I. Laskar, R. Kumar, B. Bhattacharjee, Some aspects of evaluation of concrete through mercury intrusion porosimetry, Cem. Concr. Res. 27 (1997) 93–105.
[58] M. Mindess, J.F. Young, D. Darwin, Concrete, second ed. Prentice Hall, New Jersey, 2003.
[59] P. Halamickova, R.J. Detwiler, D.P. Bentz, D.J. Garboczi, Water permeability and chloride ion diffusion in Portland cement mortars: relationship to sand content and critical pore diameter, Cem. Concr. Res. 25 (1995) 790–802.
[60] F. Khaddour, D. Gregoire, G. Pijaudier-Cabot, Computing permeation properties of mortar from pore size distribution, in: Bicanic, et al., (Eds.), Computational Modelling of Concrete Structures, Taylor & Francis Group London 2014, pp. 405–414.
[61] NT BUILD 492, Concrete, Mortar and Cement-Based Repair Materials: Chloride Migration Coefficient from Non-Steady-State Migration Experiments, NORDTEST, Espoo, 1990.
[62] C. Lu, Y.W. Mai, Influence of aspect ratio on barrier properties of polymer-clay nanocomposites, Phy. Rev. Let. 95 (2005) 088303.
[63] J. Li, J.K. Kim, Percolation threshold of conducting polymer composites containing 3D randomly distribution graphite nanoplatelets, Compos. Sci. Technol. 67 (2007) 2114–2120.
[64] L.E. Nielsen, Models for the permeability of filled polymer systems, J. Macromol. Sci. Chem. A 1 (1967) 929–942.
[65] R.K. Bharadwaj, Modelling the barrier properties of polymer-layered silicate nanocomposites, Macromolecules 34 (2001) 9189–9192.
[66] O. Valenta, The permeability and durability of concrete in aggressive conditions, Proceedings of 10th International Congress on Large Dam, Montreal 1970, pp. 103–117.